Developing turbulent flow in a rotating channel

Pål J. Nilsen* and Helge I. Andersson
Department of Applied Mechanics, The Norwegian Institute of Technology, N-7034 Trondheim, Norway

An algebraic second-moment closure with rotational stress-producing terms embodied is employed in a numerical study of developing flow in the entrance region of a rotating channel. The results of the computations are compared with measurements of Koyama and Ohuchi. Reasonable agreement with their data is observed along the stabilized suction side, whereas deviations at the destabilized pressure side are ascribed to the presence of longitudinal vortical structures in the laboratory channel.

Keywords: channel flow; Coriolis forces; turbulence modeling; second-moment closure

Introduction

Turbulent flows in rotating frame of references are frequently encountered in industrial and geophysical applications. Among the many engineering applications are the flow through coolant channels in the rotor of electrical machines and in the rotating passages in turbomachinery equipment, as well as the boundary layers on helicopter rotor blades. Because the engineering approach to fluid flow calculations in the foreseeable future will be based on the Reynolds-averaged Navier-Stokes equations, the success of computerized flow analysis relies heavily on the turbulence closure model embodied in the actual software. Unfortunately, the widely used $k-\varepsilon$ model, like any other turbulence model based on Boussinesq's eddy viscosity hypothesis, is unable to mimic the experimentally observed effects of the Coriolis forces on the turbulence field. Second-moment closures derived from the exact transport equations for the individual Reynolds stress components are, conversely, automatically accounting for body forces resulting from buoyancy, curvature and system rotation. Launder et al. (1987), for instance, computed the fully developed flow in a plane channel rotating in orthogonal mode and reproduced the main effects of rotation observed experimentally. Launder et al. (1987) applied a differential Reynolds stress model (RSM) in their study, whereas the present authors (Andersson and Nilsen 1989) derived an algebraic stress model (ASM) for rotating flows, which represents a compromise between RSM closures and two-equation transport models of the $k-\varepsilon$ type. This ASM model, which explicitly includes Coriolis-force terms, is based on the principle of material frame-indifference addressed, for instance, by Thomas and Takhar (1988). The model has recently been applied by Nilsen and Andersson (1990) to compute the turbulent flow over a backward-facing step in spanwise rotation.

The objective of the present study is to demonstrate the performance of the frame-invariant ASM closure in a computation of the flow in the entrance region of a plane channel in spanwise rotation. The developing wall boundary layers and the potential core will be computed simultaneously with an elliptic solver, thereby providing a more general treatment than the parabolic boundary layer approach adopted by Masuda et al. (1983), in which the velocity distribution in the free stream was prescribed in accordance with measured velocity data. Comparisons will be made with experimental data of Koyama and Ohuchi (1985).

Mathematical modeling

The problem considered is that of steady, incompressible and fully turbulent flow between two parallel walls in spanwise rotation, as schematically shown in Figure 1. The Reynolds-averaged equation governing the transport of mean momentum is expressed in a rotating Cartesian frame of reference as

$$\rho \frac{\partial (U_j U_i)}{\partial x_j} = -\frac{\partial P}{\partial x_i} + \frac{\partial}{\partial x_j}\left(\mu \frac{\partial U_i}{\partial x_j} - \rho \overline{u_i u_j}\right) - 2\rho \epsilon_{ijk} \Omega_j U_k \qquad (1)$$

subject to the continuity constraint $\partial U_i/\partial x_i = 0$.

An algebraic model for the unknown Reynolds stresses $-\rho\overline{u_i u_j}$ is obtained from a transport equation for the second-moments $\overline{u_i u_j}$

$$C_{ij} = G_{ij} + D_{ij} + \phi_{ij} - \varepsilon_{ij} \qquad (2)$$

where the various physical processes tending to change $\overline{u_i u_j}$ are represented symbolically. Following Andersson and Nilsen (1989), a frame-invariant formulation of the convective derivative

$$C_{ij} = \frac{D\overline{u_i u_j}}{Dt} - \tfrac{1}{2} R_{ij} \qquad (3)$$

is adopted, in accordance with the principle of material frame-indifference as discussed by Thomas and Takhar (1988). Hence, with half of the rotational stress generation R_{ij} assigned to the convective derivative, the Coriolis contribution to the total stress generation is correspondingly reduced, that is,

$$G_{ij} = P_{ij} + \tfrac{1}{2} R_{ij} \qquad (4)$$

Rodi (1976) demonstrated that the differential equation (Equation 2) can be converted into an algebraic model

*Present address: DNV Technica, P.O. Box 300, N-1322 Høvik, Norway.

Address reprint requests to Professor Andersson at the Department of Applied Mechanics, The Norwegian Institute of Technology, N-7034 Trondheim, Norway.

Received 13 September 1991; accepted 20 September 1993

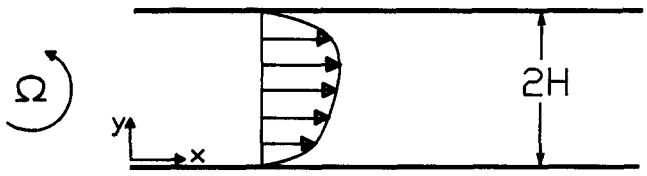

Figure 1 Schematic of flow configuration and coordinate system

expression if the net transport of $\overline{u_i u_j}$ is assumed to be proportional to the net transport of the mean turbulent kinetic energy k. A generalization of Rodi's hypothesis to flows subject to system rotation was proposed more recently by Andersson and Nilsen (1989):

$$C_{ij} - D_{ij} = \frac{\overline{u_i u_j}}{2k}(C_{kk} - D_{kk}) = \frac{\overline{u_i u_j}}{2k}(P_{kk} - \varepsilon_{kk}) \tag{5}$$

where the latter equality follows from contraction of the indices in Equation 2, recognizing that $\phi_{kk} = R_{kk} = 0$.

Finally, the dissipation rate ε_{ij} of the Reynolds stresses is assumed to be locally isotropic, whereas the pressure–strain correlation ϕ_{ij} is split into three different parts and modeled separately. Following Launder et al. (1987), the linear return-to-isotropy model is retained for the purely turbulent interactions, whereas interactions of mean strain and rotation with fluctuating quantities are approximated by a rotating-flow version of the isotropization-of-production model. The effect of turbulent pressure reflections from the walls, that is, ϕ_{ij}^w, is also modeled in accordance with Launder et al. (1987).

With these modeling assumptions introduced in Equation 2, the original differential equation can be expressed in algebraic form as

$$\frac{\overline{u_i u_j}}{k} - \frac{2\delta_{ij}}{3} = \frac{(1 - C_2)(P_{ij} - \frac{1}{3}\delta_{ij}P_{kk} + \frac{1}{2}R_{ij}) + \phi_{ij}^w}{\frac{1}{2}P_{kk} + \varepsilon(C_1 - 1)} \tag{6}$$

where the constants C_1 and C_2 take the values 1.8 and 0.6, respectively. It is noteworthy that the original ASM model from Rodi (1976) is recovered in the nonrotating case if the wall-correction ϕ_{ij}^w is neglected. Moreover, according to common practice, the mean kinetic energy of the turbulence, k, and its dissipation rate, ε, appearing in the ASM model (Equation 6) are obtained from their own transport equations. It is important to notice that there are no explicit influences of rotation in these differential equations for k and ε.

The numerical calculations reported herein were made with an adapted version of the elliptic finite-volume solver TEAM-ASM described by Huang and Leschziner (1983). The ASM model (Equation 6) was implemented consistently with the stability-promoting measures discussed by Huang and Leschziner (1985). Nevertheless, fairly strong underrelaxation of the Reynolds stress components was required in the iterative matrix solver to achieve converged solutions.

The ASM-model (Equation 6) is not applicable directly into the walls, and the wall-function approach was therefore adopted to bridge the near-wall sublayer. Inlet boundary conditions were prescribed in accordance with measured distributions of U and $\overline{u^2}$, whereas fully developed flow conditions were imposed at the outflow boundary. However, to ensure parallel streamlines at the outlet, the length of the calculation domain was three times the length of the experimental test section (i.e., 2,000 mm rather than 670 mm).

Numerical results and discussion

Calculations were carried out for two different cases with the bulk mean velocity $U_m = 10$ m/s, namely, $\Omega = 0$ rad/s and $\Omega = -10$ rad/s (i.e., -300 rpm). The results to be presented herein are for the latter case, which characterizes by a bulk Reynolds number $Re = 11{,}800$ and a rotation number $Ro = -0.12$. The rectangular calculation domain, with dimensions 2,000 mm × 40 mm, was divided into 90 × 32 cells. Because $\Omega < 0$, the two channel walls at $y = 0$ and $y = 40$ mm are becoming the *suction* and *pressure* sides, respectively.

Computed profiles of the mean velocity U and the streamwise turbulence intensity $(\overline{u^2})^{1/2}$ at three different streamwise positions are presented in Figures 2 and 3, respectively, whereas the streamwise variation of the friction velocity U_* is shown in Figure 4. The numerical results are compared with experimental findings of Koyama and Ohuchi (1985). A hot-wire system was used for the measurements of the mean velocity and the Reynolds stresses in the straight test section (aspect ratio 7:1) of their rotating wind tunnel, and a Preston tube was used to obtain the wall shear stress.

It is readily observed from the displayed results that the boundary layers along the channel walls thicken in the streamwise direction at the expense of the shrinking potential core. The predicted growth of the boundary layers is, however, somewhat underestimated in comparison with the experimental

Notation

C_1, C_2	model constants
C_{ij}	convection of Reynolds stresses
D_{ij}	diffusion of Reynolds stresses
G_{ij}	total production of Reynolds stresses
H	channel half-width
k	mean turbulent kinetic energy, $\overline{u_i u_i}/2$
P	reduced pressure, $p - \rho\Omega^2 x_i x_i/2$
P_{ij}	mean shear production, $-\left(\overline{u_i u_k}\frac{\partial U_j}{\partial x_k} + \overline{u_j u_k}\frac{\partial U_i}{\partial x_k}\right)$
R_{ij}	rotational production, $-2\Omega_k[\overline{u_j u_m}\epsilon_{ikm} + \overline{u_i u_m}\epsilon_{jkm}]$
Re	Reynolds number, $\rho U_m H/\mu$
Ro	rotation number, $2H\Omega/U_m$
$\overline{u_i u_j}$	kinematic Reynolds stress
U_c	centerline velocity
U_i	mean velocity component in x_i-direction
U_m	bulk mean velocity
U_*	wall friction velocity, $(\tau_w/\rho)^{1/2}$
x_i	Cartesian coordinate
x, y	coordinates defined in Figure 1

Greek letters

δ_{ij}	Kronecker delta
ε	energy dissipation rate, $\varepsilon_{ii}/2$
ε_{ij}	dissipation rate tensor, $2\delta_{ij}\varepsilon/3$
ϵ_{ijk}	Levi-Civita symbol
μ	dynamic viscosity
ρ	density
τ_w	shear stress at the wall, $\mu\partial U/\partial y\|_w$
ϕ_{ij}, ϕ_{ij}^w	pressure-strain model
Ω_i	angular velocity

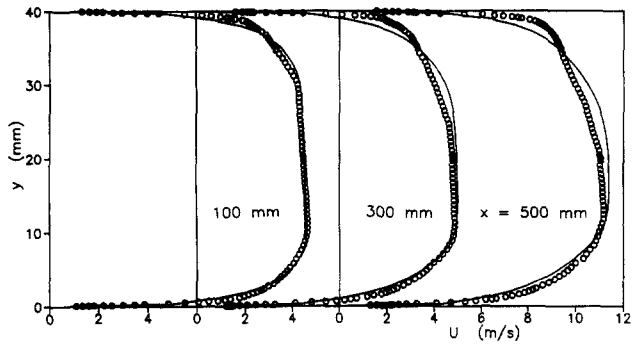

Figure 2 Profiles of streamwise mean velocity component U at three different locations for Ro = −0.12; computed results (*lines*) are compared with experimental data (*symbols*) of Koyama and Ohuchi (1985)

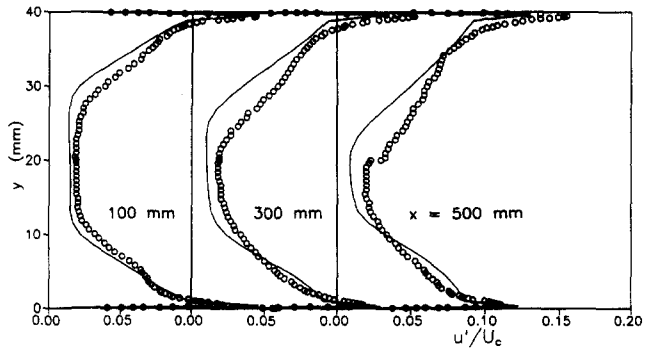

Figure 3 Profiles of streamwise turbulence intensity $u' = (\overline{u^2})^{1/2}$ at three different locations for Ro = −0.12 (legend as in Figure 2)

data. It may be worthwhile to mention that, according to the computations, the wall boundary layers tend to the merge at about $x = 800$ mm and, eventually, fully developed flow conditions are established downstream of $x = 1{,}500$ mm. This observation suggests that the flow at the downstream measuring station ($x = 500$ mm) is far from being fully developed.

More interestingly, perhaps, is the striking difference in the growth of the two boundary layers. The promoted boundary layer development along the pressure side contrasts with the suppressed growth at the suction side. This striking effect of the Coriolis force is, at least qualitatively, reproduced in the computer simulation. However, the results compare more favorably with the experimental data along the suction side than near the pressure wall. This can be ascribed to the experimentally observed counter-rotating Taylor-Görtler-like vortices on the pressure side, which cannot be reproduced by a two-dimensional mathematical model. Obviously, highly turbulent fluid is being conveyed from the pressure side and out into the center by these unsteady vortical roll-cells, whose motion also contributes directly to the measured turbulent stresses, thereby explaining the significant discrepancies in the upper half of Figure 3. This particular issue has recently been addressed in some detail by Kristoffersen and Andersson (1993).

The differing boundary layer development along the two walls is obviously associated with the difference in the turbulence levels near the stabilized suction side and the destabilized pressure side. However, according to the change of sign of the rotational production $R_{11} \approx 4\Omega\overline{uv}$ across the

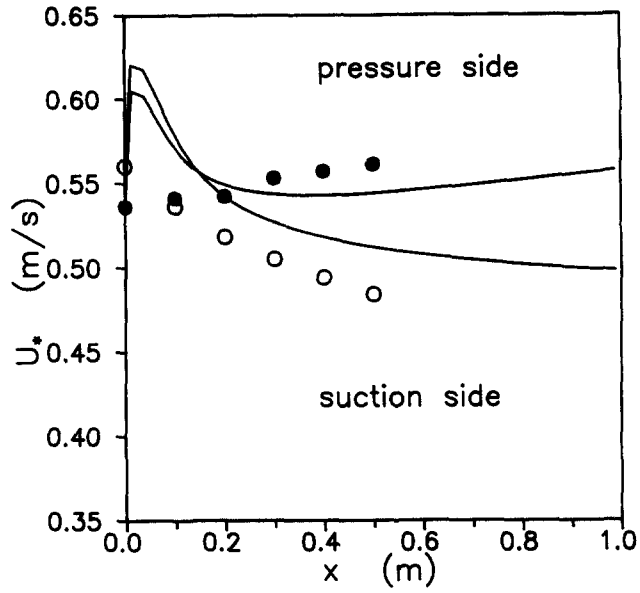

Figure 4 Streamwise variation of the wall friction velocity U_* for Ro = −0.12 (legend as in Figure 2)

channel, just the opposite behavior should have been expected. The observed effect of system rotation on $\overline{u^2}$ is therefore an *indirect* one, which stems from rotational production of $\overline{v^2}$. Because $R_{22} = -R_{11}$, negative rotation tends to reduce $\overline{v^2}$ near the suction side with a corresponding enhancement at the pressure side. These changes in $\overline{v^2}$, and accordingly in the magnitude of the mean shear production $P_{12} \approx -\overline{v^2}\partial U/\partial y$ and $\overline{uv}$, indirectly result in corresponding changes in the mean shear production $P_{11} \approx -2\overline{uv}\partial U/\partial y$ and thus in $\overline{u^2}$. The observed results in Figure 3 therefore suggest that the direct rotational contribution to $\overline{u^2}$ by means of R_{11} is far outweighed by the indirect changes in P_{11}.

Conclusion

The promoted boundary layer development along the destabilized pressure side and the suppressed growth at the stabilized suction side of a rotating channel have been reproduced, at least qualitatively, by the generalized ASM closure for Ro = −0.12. At this particular rotation number, the overall influence of the Coriolis force is ascribed to the indirect influence of the rotational generation of the transverse stress component $\overline{v^2}$.

Acknowledgment

The authors are grateful to Dr. H. S. Koyama for clarifying discussions and for generously providing the experimental data in tabulated form.

References

Andersson, H. I. and Nilsen, P. J. 1989. Comparison of algebraic Reynolds stress models for rotating flows. *ASME Forum on Turbulent Flows*, **76**, 13–18

Huang, P. G. and Leschziner, M. A. 1983. An introduction and guide to the computer code TEAM. UMIST Mech. Eng. Dept. Rep. TDF/83/9/(R)

Huang, P. G. and Leschziner, M. A. 1985. Stabilization of recirculating-flow computations performed with second-moment closures and third-order discretization. *Proc. 5th Symp. Turbulent Shear Flows*, Ithaca, 20.7–20.12

Koyama, H. S. and Ohuchi, M. 1985. Effects of Coriolis force on boundary layer development. *Proc. 5th Symp. Turbulent Shear Flows*, Ithaca, 21.19–21.24

Kristoffersen, R. and Andersson, H. I. 1993. Direct simulations of low Reynolds number turbulent flow in a rotating channel. *J. Fluid Mech.*, **256**, 163–197

Launder, B. E., Tselepidakis, D. P. and Younis, B. A. 1987. A second-moment closure study of rotating channel flow. *J. Fluid Mech.*, **183**, 63–75

Masuda, S., Koyama, H. S. and Ariga, I. 1983. High Reynolds number turbulence model of rotating shear flows. *Bull. JSME*, **26**, 1534–1541

Nilsen, P. J. and Andersson, H. I. 1990. Rotational effects on sudden-expansion flows. *Engineering Turbulence Modelling and Experiments*. Elsevier, New York, 65–72

Rodi, W. 1976. A new algebraic relation for calculating the Reynolds stresses. *ZAMM*, **56**, T219–T221

Thomas, T. G. and Takhar, H. S. 1988. Frame-invariance of turbulence constitutive relations. *Astrophys. Space Sci.*, **141**, 159–168